Annals of Glaciology

Article

Cite this article: Li Y, Fan X, Talalay PG, Dou Y, Lu S, Kang S, Li X, Hong J (2021). Shallow hot-point drill system for active layer temperature measurement along Zhongshan–Dome A traverse, Antarctica. *Annals of Glaciology* **62** (84), 157–165. https://doi.org/10.1017/aog.2020.87

Received: 17 April 2020
Revised: 11 December 2020
Accepted: 14 December 2020
First published online: 18 January 2021

Key words:
Hot-point drill; ice drilling; penetration rate; snow–firn temperature; thermal equilibrium

Author for correspondence:
Jialin Hong, E-mail: hjl2398@126.com

© The Author(s), 2021. Published by Cambridge University Press. This is an Open Access article, distributed under the terms of the Creative Commons Attribution licence (http://creativecommons.org/licenses/by/4.0/), which permits unrestricted re-use, distribution, and reproduction in any medium, provided the original work is properly cited.

cambridge.org/aog

Shallow hot-point drill system for active layer temperature measurement along Zhongshan–Dome A traverse, Antarctica

Yazhou Li[1], Xiaopeng Fan[1,2], Pavel G. Talalay[1], Yinke Dou[3], Siyu Lu[1], Shichang Kang[2], Xiao Li[1] and Jialin Hong[1]

[1]Polar Research Center, Jilin University, Changchun, Jilin 130021, China; [2]State Key Laboratory of Cryospheric Science, Northwest Institute of Eco-Environment and Resources, Chinese Academy of Sciences, Lanzhou 730000, China and [3]College of Electrical and Power Engineering, Taiyuan University of Technology, Taiyuan 030024, China

Abstract

In glaciology, snow–firn temperature at 10 m is considered a representation of the mean annual air temperature at the surface (MAAT) of the studied site. Although MAAT is an important parameter in ice-sheet investigations, it has not been widely measured in Antarctica. To measure the 10 m snow–firn temperature in Antarctica, a shallow hot-point drill system is designed. In this simple and lightweight system, a hot-point drill can melt boreholes with a diameter of 34 mm in the snow–firn to a depth of 30 m and a temperature sensors string can measure the borehole temperature precisely. In the 2018/19 field season, 16 boreholes along the Zhongshan–Dome A traverse were drilled, and the borehole temperature was measured. Although certain problems existed pertaining to the hot-point drill, a total depth of ~244 m was successfully drilled at an average penetration rate of ~10 m h^{-1}. After borehole drilling, ~12–15 h were generally required for the borehole to achieve thermal equilibrium with the surroundings. Preliminary results demonstrated that the 10 m snow–firn temperature along the traverse route was affected by the increasing altitude and latitude, and it decreased gradually with an increase in the distance from Zhongshan station.

1. Introduction

As an important parameter in ice-sheet investigation, mean annual air temperature at the surface (MAAT) is an indicator of the thermal state of the local climate. It is generally accepted that the snow–firn temperature measured at a 10 m depth is a close approximation of the MAAT (Mock and Weeks, 1966; Loewe, 1970). This makes it possible to estimate MAAT by measuring the temperature in a borehole in areas where there are no meteorological records. However, it is worth to be mentioned that the snow–firn temperature at 10 m depth cannot be always equal to MAAT, especially in the glaciers where the surface melting occurs (Zagorodnov and others, 2006). Usually, the depth of the mean annual air temperature for a given site depends on the local snow–firn properties, accumulation rate and possibly wind conditions (Zagorodnov and others, 2012). In several parts of Antarctica, such as Mizuho Plateau (Satow and others, 1974), Antarctic Peninsula (Reynolds, 1981) and Ross Ice Shelf (Thomas, 1976), the MAAT was measured by drilling boreholes and installing temperature sensors strings or thermistor strings. Many of the 10 m snow–firn temperature in Antarctica were measured along the traverse direction from the coast to inland in field expeditions (Morris and Vaughan, 1994; Van Den Broeke and others, 1999). Although extensive measurements of the 10 m snow–firn temperatures were performed in Antarctica, there are still large gaps in spatial coverage, especially in the interior of the Antarctic ice sheet (Wang and Hou, 2011). Multiple regression analysis is used to determine the relationship between the measured MAAT and the longitude, latitude and altitude of the studied sites (Martin and Peel, 1978; Wang and Hou, 2011). In Antarctica, the MAAT usually decreases from mid-latitude to the South Pole, from the coastal regions to inland and from sea level to high altitude.

The borehole for active layer temperature measurement can be drilled using both mechanical and thermal drills. Previously, shallow mechanical drills were commonly used, such as the SIPRE hand auger used in the Mizuho Plateau (Yamada and Narita, 1975) and the Polar Ice Coring Office lightweight corer used in Dronning Maud Land (Isaksson and others, 1996). Comparing with hand auger, electromechanical corer usually has a higher penetration rate and lower power consumption. Hence, energy dissipation with hand augering is likely higher than electromechanical coring (Zagorodnov and others, 2012). To the best of our knowledge, no type of thermal drill, including hot-point drill, hot water drill or steam drill, was used in Antarctica for active layer temperature measurements.

Powered by heat elements in the thermal head at its bottom end, the electrically heated hot-point drill is widely used to drill boreholes for measuring the features of glaciers, ice caps and ice sheets, such as vertical velocity distribution, basal water pressure and snow–firn density distributions (Mathews, 1959; Hodge, 1976; Zagorodnov and others, 2013). The input power and rate of penetration (ROP) of the electrically heated hot-point drills vary across wide ranges of

Table 1. Available MAAT along Zhongshan–Dome A traverse

Time	Sites	Longitude, E	Latitude, S	Distance[a] (km)	Altitude (m)	10 m snow–firn temperature (°C)
2005–2008	LGB69	77.0747	70.8353	172	1854	−27.2
1994	LT925	77.2886	71.0954	202	1996	−28.5
1994	LT910	77.5112	71.3606	233	2135	−30.7
1994	LT895	77.7305	71.6205	263	2214	−31.7
1994	LT880	77.9509	71.8808	294	2325	−33.1
1994	LT865	77.9494	72.1505	324	2351	−33.3
1994	LT850	77.7231	72.4106	354	2424	−34.7
1994	LT835	77.4936	72.6712	384	2468	−34.5
1994	LT805	77.0268	73.1914	444	2581	−36.1
1994	LT790	76.7877	73.452	474	2537	−36.1
1994	LT743	76.1687	74.2595	564	2476	−35.6
1994	LT730	75.8756	74.4793	594	2468	−35.5
2005–2008	EAGLE	77.0239	76.4197	801	2830	−43.1
2005–2008	Dome A	77.3439	80.3675	1248	4093	−58.2

[a]Distance to the coast.

0.22–8 kW and 0.8–25 m h^{-1}, respectively (Talalay, 2020). Most hot-point drills demonstrate a diameter of 30–80 mm, while the minimum diameter can be as low as 18 mm and the maximum diameter can reach 150 mm (Ignatov, 1960; Gillet, 1975). The hot-point drills designed for drilling in cold ice usually have a bailer to remove the meltwater out of the borehole, such as the BGR Ice Drill (Zeibig and Delisle, 1994). When drilling in snow–firn, the bailer becomes unnecessary as the melted water can percolate into the pores of the surrounding environment. An additional centralizer on the hot-point drills can prevent tilting in deep borehole drilling (Zagorodnov and others, 2014). When compared to mechanical drills, the hot-point drills have a simpler structure, lighter weight and shorter setup/down time. More importantly, the hot-point drills require less manual labor and are easier to operate in the harsh environment of Antarctica.

Since the Chinese National Antarctic Research Expedition (CHINARE) started its inland expedition along Zhongshan–Dome A traverse, several types of glaciological surveys were conducted, such as the measurements of accumulation rate, ice velocity and surface mass balance (Qin and others, 2000; Zhang and others, 2008; Ding and others, 2015). However, the temperature measurements along the traverse were limited and the MAAT is still largely unknown. In Dome A, an averaged modeled surface temperature of −57.7°C and a measured temperature of −58.2°C at 10 m depth were reported by Chen and others (2010). In addition, the CHINARE and Australian National Antarctica Research Expedition measured the MAAT along Zhongshan–Dome A traverse at 14 sites by borehole drilling method or automatic weather station observation (Ding and others, 2010). All available 10 m snow–firn temperatures along Zhongshan–Dome A traverse are listed in Table 1. It can be seen that most of the MAAT is measured below the latitude of 76°S. The temperature data from 76° S to 80°S are scarce. To fill in the gap, we design a shallow hot-point drill system and it was used for active layer temperature measurement along the Zhongshan–Dome A traverse.

2. Methodology

2.1. Shallow hot-point drill system

As shown in Figure 1a, the shallow hot-point drill system contains several parts: a commercially available gasoline generator and transformer, a hand winch with an electric slip ring, a stand with a support arm and pulley, a hot-point drill suspended by an armored cable and a temperature measurement system. The shallow hot-point drill system weighs ~30 kg (without generator) and can be handled by one person.

The Honda EU20i gasoline generator is used to produce 220 V AC with a maximum power of 1.6 kW (Fig. 1b). The fuel tank capacity of the generator is 3.6 L. When one-fourth of the load of the generator is used, the fuel consumption is 0.44 L h^{-1}. Depending on the power consumption, the generator with a full fuel tank can be operated for 3.4–8.2 h without refueling. The transformer is $TDGC_2$-5KVA type with a rated current of 10 A (Fig. 1c). The input voltage for the transformer was 220 V, while the output voltage was adjustable from 0 to 500 V. The size of the transformer is 23 cm × 28.5 cm × 23 cm and the weight is 15 kg. During the drilling process, the generated 220 V AC by the Honda generator is transferred to the transformer, which is then transformed to 360 V to provide power for the hot-point drill.

The commercially available hand winch is used to lift and lower the hot-point drill using a cable wound on its drum (Fig. 1d). It consists of a drum, handle, gear-driven system and base. The maximum pull force for the hand winch is 5.3 kN and it can hold 5.2 mm diameter cable at the maximum length of 30 m. While drilling in the snow–firn, the hand winch should be fixed on the stand and its handle is driven by the operator according to the ROP of the hot-point drill. A slip ring is installed on the side of the hand winch to prevent the rotation of the electric cable from the transformer along with the drum. The electric slip ring has a diameter of 69 mm and a maximum current of 10 A.

In the field, a stand with a fixed support arm and pulley acts as a simple crane to hoist the hot-point drill. In this study, the stand was ~1 m in height and it had steel legs and a wooden desktop. During drilling, the hand winch and transformer were fixed on top of the stand.

The hot-point drill can drill the boreholes by melting snow–firn with its heated thermal head at the bottom of the drill. The power for the hot-point drill is supplied by a 5.2 mm diameter cable. The cable with a rated current of 15 A is armored using Kevlar and can withstand a maximum pull force of 15 kN. The hot-point drill has a diameter of 30 mm and a length of ~0.9 m. The weight of the drill is ~3.5 kg. As shown in Figure 2, the hot-point drill contains three parts: a thermal head, a drill body and a cable termination. Each part is connected with another part through a steel connector.

The thermal head consists of a copper shell, a cartridge heater and a short steel tube. The conical copper shell has a diameter of 34 mm to ensure a minimum clearance of 2 mm between the drill body and the borehole wall. The customized cartridge heater is 8 mm in diameter and 110 cm in length. It has three different sections from the bottom to the top: heated, non-heated and waterproof parts. The heated part is 75 mm in length while the non-heated part is 10 mm. With a larger diameter of 18 mm, the waterproof part can ensure that the cartridge heater works under a water pressure of 0.5 MPa. The rated power and voltage of the cartridge heater are 1000 W and 360 V, respectively. Owing to its low thermal conductivity, the steel tube can prevent the upward transfer of the heat generated by the cartridge heater.

The drill body contains an aluminum tube and nine lead dead weights. Each dead weight weighs 0.2 kg.

Cable termination was modified according to the cable termination of a DJ1031-type commercial geological logger (http://www.gi200.com/index.php/default/content/10278.html). In our design, a 'weak point' was added to ensure that the cable and the cable termination can be saved if the lower part of the hot-point drill is stuck tightly in the borehole. The 'weak point' consists of a socket, a pin, a plug, a connecting tube and four screws. The lower part of the plug is fixed on the connecting tube by the

https://doi.org/10.1017/aog.2020.87 Published online by Cambridge University Press

Fig. 1. Overview of (a) shallow hot-point drill system; (b) gasoline generator; (c) transformer; (d) hand winch.

four screws while its upper part is inserted in the socket and locked by a small pin. The connecting tube has no connection with the upper components. The 4 mm pin is manufactured using Teflon and can be broken under a pulling force exceeding 2 kN.

The temperature measurement system contains a 50 m long temperature sensors string and a data acquisition system. All the systems are powered using a 12 V, 25 Ah lead acid battery. The temperature sensors string with a diameter of 15 mm consists of 50 temperature sensors and a cable. All the temperature sensors are attached to the cable with 1 m increment. The temperature sensor has a measurement range of ~−50 to 50 °C and a precision of ±0.2 °C. Each temperature sensor consists of a flexible circuit board, which is then covered by a thick-walled heat shrinkable tube. The weight of the temperature sensors string is supported by the cable when it is used. At the bottom end of the cable, an additional dead weight is added to maintain the chain vertically in the borehole. The data acquisition system can collect the data from the temperature sensors string every 10 min and then store them in a secure digital card.

2.2. Drilling and measurements

The borehole drilling and active layer temperature measurements were conducted in the 2018/19 field season of the 35th CHINARE along the Zhongshan–Dome A transverse, East Antarctica (Fig. 3). On 18 December 2018, the CHINARE inland team started their trip from Zhongshan station to Kunlun station using vehicles. After 18 d, the inland team arrived at Kunlun station. There were ten campsites during the trip, and in seven of them, the active layer temperature was measured. The inland team left Kunlun station on 24 January 2019 and arrived at the departure base of Zhongshan station on 8 February 2019. During the return trip, the active layer temperature measurements were performed in nine campsites. The detailed description of the 16 measurement sites is listed in Table 2.

The borehole drilling and temperature measurement were only performed when the inland team arrived at the campsites. Before drilling a hole, the snow surface was leveled to ensure the stand was horizontal. Then, the thermal head of the hot-point drill was heated by adjusting the voltage between 180 and 200 V. After the thermal head became hot, the hot-point drill was lowered using the hand winch to melt the snow–firn. When the thermal head was completely in the snow–firn, the voltage was increased to 330 V, which corresponded to a power of 890 W. Because of the high porosity of snow–firn, the meltwater percolated quickly; consequently, the borehole remained dry during drilling. Once the borehole was completed and the hot-point was lifted to the surface, the temperature sensors string was installed for the total length of the borehole and the data acquisition operation was started. To reduce the influence of surface air on the borehole temperature, the wellhead was covered by snow. Temperature measurement continued until the inland team left the campsite. The fieldwork was limited by the time available during the overnight stops except in the DT349 site, Taishan and Kunlun stations. In most cases, the time for temperature measurement was <16 h (Table 2).

3. Results and discussion

3.1. Performance of hot-point drill

To study the hot-point drilling performance, a drilling experiment was conducted in the DT259 site. The voltage of the thermal head was changed to investigate the effect of the power of the drill head on ROP. The voltage was varied to 150, 200, 250, 300 and 330 V, which corresponded to the power values of 184, 326, 518, 729 and

https://doi.org/10.1017/aog.2020.87 Published online by Cambridge University Press

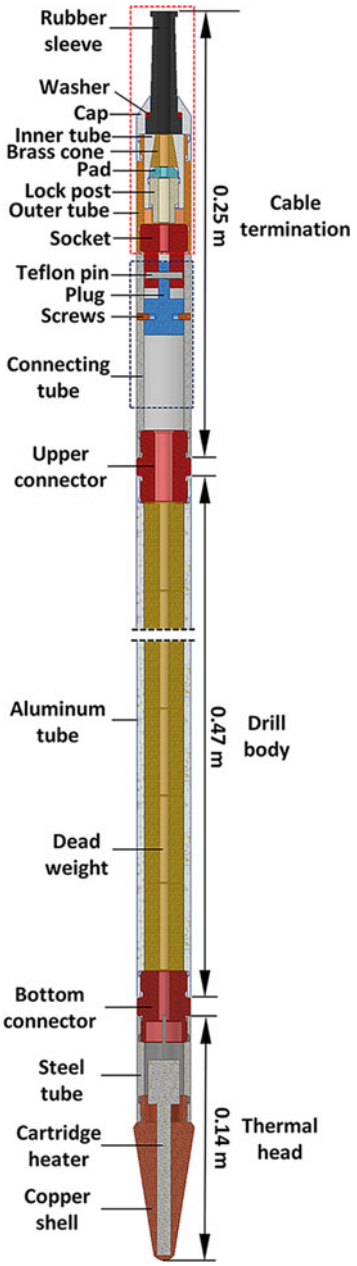

Fig. 2. Schematic of the shallow hot-point drill. Structure of the commercial cable termination is indicated by the red box; 'weak point' is indicated by the blue box.

890 W, respectively. For each power value, the thermal head was used to drill to a depth of 3 m from the surface. The ROP was calculated in increments of 10 cm by recording the depth and time. It can be observed that the ROP increased linearly with an increase in input power (Fig. 4). When the power changed from 184 to 890 W, the ROP increased from 4.0 to 18.1 m h^{-1}.

The penetration rate of a hot-point drill depends on the density of the active layers that are melted. In the DT259 site, a 16 m deep borehole was also drilled using a constant power of 890 W to observe the change in ROP with borehole depth. The ROP was calculated using the aforementioned method with the exception that the depth increments were chosen to be 1 m instead of 10 cm. The ROP decreased from 16.3 m h^{-1} at the surface to 9.5 m h^{-1} at the bottom of the borehole and the average ROP of the borehole was 12.5 m h^{-1} (Fig. 4). The snow–firn density obtained in a pit of the site increased from 420 kg m^{-3} at the surface to 560 kg m^{-3} at a depth of 2.5 m. According to the heat transfer theory of hot-point drills, there exists a linear relationship between snow–firn density and the ROP (Aamot, 1967; Ulamec and others, 2007). Considering this fact, it is speculated that the ROP decrease with depth was caused by increased snow–firn density.

In total, 17 boreholes with depths more than 10 m were drilled. Sixteen of these boreholes were used for active layer temperature measurements; moreover, the drilling process in a borehole at Taishan station was stopped at a depth of 10 m because the hot-point drill became stuck in the borehole. This accident occurred due to the tilting of the hot-point drill. The maximum depth was 21 m while most of the boreholes were either 13 or 16 m. The ROP changed from ~15 m h^{-1} at the surface to ~7.5 m h^{-1} at 20 m. In general, a borehole with a depth of 16 m required a drilling time of 1.5–2 h. When drilling in snow–firn, the meltwater percolated away and the diameter of the borehole was almost the same as the diameter of the thermal head.

In general, the shallow hot-point drill performed well; however, the following problems occurred, which can be improved in the future:

(a) Because of its light weight, the hot-point drill easily tilted in the opening of the borehole. In the field, sometimes the driller had to lift the hot-point drill to a certain height and then release it suddenly to make the hot-point drill penetrate a certain depth in snow–firn. To overcome this problem, it is better to increase the weight of the hot-point drill in the future by adding more dead weights. Another option is to add a guide tube in the system so that the hot-point drill can drill along the tube in the opening of the borehole.
(b) While drilling downward, the hot-point drill became stuck in the boreholes several times because of borehole tilting and the refreezing of the water at the top part of the hot-point drill. Although most of the meltwater percolated into the pores of the surrounding snow–firn, small amounts of moisture covered the borehole wall. Even a marginal tilt in the hot-point drill caused its top part to touch the wet borehole wall, which then caused water to refreeze on it. With increased refreezing of water, the outer diameter of the hot-point drill became bigger than that of the thermal head. In this case, the drilling had to be stopped and the hot-point drill was lifted to the surface to remove the refrozen water. In the worst cases, the hot-point drill had to be lifted every 2–3 m during drilling. There are three methods to prevent the sticking of the hot-point drill. The first method is to increase the clearance between the borehole wall and the hot-point drill. A minimum clearance of 4 mm is suggested, which requires a diameter of 38 mm for the thermal head. Heating the side walls of the hot-point drill can be another option. The third method is to cover the side wall with a hydrophobic coating or to add a plastic cover on the aluminum body of the hot-point drill.

The hot-pint drill can also become stuck when it is lifted out of the borehole because of borehole tiling. To avoid this situation, the thermal head was usually heated using a power of 184 W during lifting.

(a) Although the rated voltage of the cartridge heater was 360 V, three cartridge heaters burned out when the voltage raised to 340 V. In the field, it was impossible to increase the ROP of the hot-point drill by inputting more power to it because the maximum voltage had to be limited to 330 V. In the future, a cartridge heater with higher rated voltage and better quality should be used.
(b) There was no load sensor or a motor in the shallow hot-point drill system; therefore, the control of the hot-point drill during drilling completely relied on the driller, which was time-consuming and laborious. An automatic drilling system may be a good choice for the harsh Antarctic environment.

https://doi.org/10.1017/aog.2020.87 Published online by Cambridge University Press

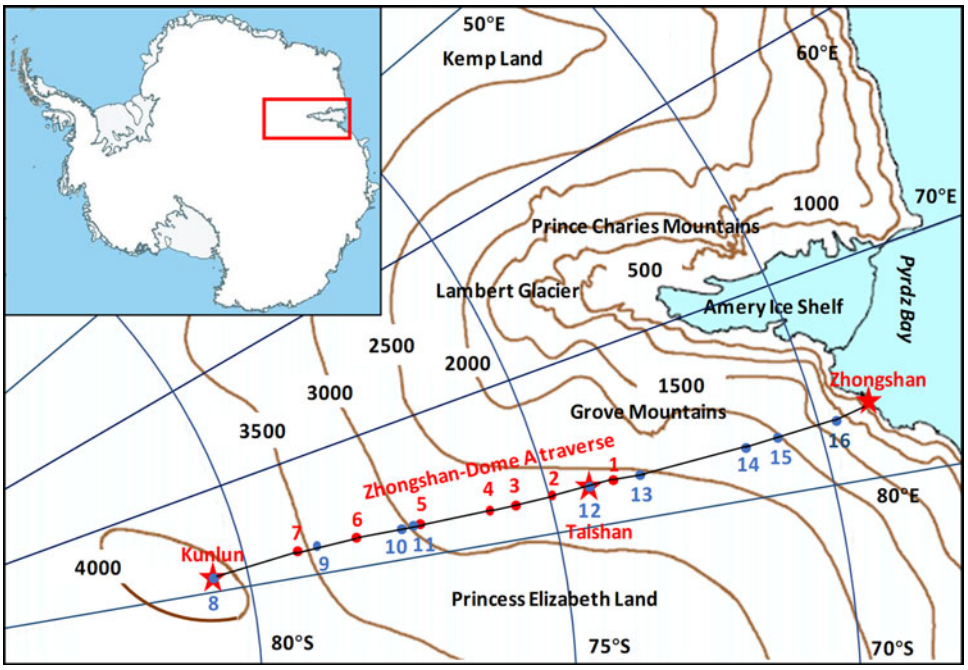

Fig. 3. Map showing the Zhongshan–Dome A traverse route and location of measurement sites. Red and blue solid dots denote the measurement sites in the direct and return trips, respectively; red stars indicate the Chinese research stations. The measurement sites are numbered using Arabic numerals.

Table 2. Description of the measurement sites

No.	Date (YYYYMMDD)	Sites	Longitude, E	Latitude, S	DFZS[a] (km)	Altitude (m)	Borehole depth (m)	Measurement time (h)
1	20181223	DT086	77°00′25″	73°28′09″	464	2540	21	10
2	20181227	DT171	76°57′59″	74°51′17″	630	2777	13	10.2
3	20181228	DT221	76°48′10″	75°47′50″	734	2771	13	12.7
4	20181229	DT253	77°01′50″	76°21′14″	798	2815	16	13
5	20181230	DT299	76°57′37″	77°10′58″	890	2960	16	9.3
6	20181231–20190101	DT349	77°04′36″	78°03′13″	990	3170	16	32.5
7	20190102	DT402	76°59′27″	79°00′50″	1100	3729	13	9.3
8	20190118	Kunlun	77°06′41″	80°25′04″	1260	4086	16	43.6
9	20190125	DT391	77°01′56″	78°49′29″	1074	3604	13	8.2
10	20190127	DT276	77°01′28″	76°46′27″	844	2877	13	10
11	20190128	DT259	77°02′13″	76°28′11″	810	2821	16	15.7
12	20190131–20190203	Taishan	76°58′43″	73°51′48″	520	2626	16	31
13	20190203	DT071	77°11′03″	73°07′51″	433	2600	13	11.7
14	20190205	LT884	77°53′15″	71°48′39″	283	2288	13	9.5
15	20190206	LT926	77°16′15″	71°04′39″	201	1992	10	10.8
16	20190207	LT982	76°34′42″	70°05′42″	89	1246	13	12.2

[a]Distance from Zhongshan station.

3.2. Thermal equilibrium in boreholes

As shown in Figure 5, the measured 10 m snow–firn temperature in the borehole was quite high when the temperature sensors string was initially placed in the borehole after drilling. Then, the temperature exponentially decreased with time and finally became constant. Theoretically, it is impossible for the temperature to return completely to undisturbed conditions. However, after a certain amount of time, the borehole temperature will change to a value sufficiently close to the temperature of the undisturbed formation. In our case, equilibrium with surrounding snow–firn temperature was achieved only when the decreasing rate of temperature was <0.2°C h^{-1}. According to the measured data, the thermal recovery time in the boreholes was ~12–15 h. As listed in Table 1, the measurement time at nine sites was <12 h; consequently, the measured active layer temperature in these sites was not as precise as in other sites. In the future, the temperature sensors string should be retained in the borehole for a longer amount of time until thermal equilibrium is achieved.

There are two reasons for the significantly long time required to achieve thermal equilibrium in the boreholes. First, the meltwater with a large amount of heat increased the initial snow–firn temperature. Second, the installation of the temperature sensors string can result in air convection in the borehole and consequently influence the temperature distribution in the borehole.

To evaluate the contribution of these factors, the following experiment was conducted in the 16 m deep borehole at Taishan station. The temperature sensors string was lowered into the borehole as soon as the drilling was completed. After ~31 h, the temperature sensors string was lifted out from the borehole and placed on the surface until all the sensors showed the same temperature as the surrounding air temperature. Then, the temperature sensors string was placed in the borehole again for another 15 h. The measured temperatures of all the sensors

https://doi.org/10.1017/aog.2020.87 Published online by Cambridge University Press

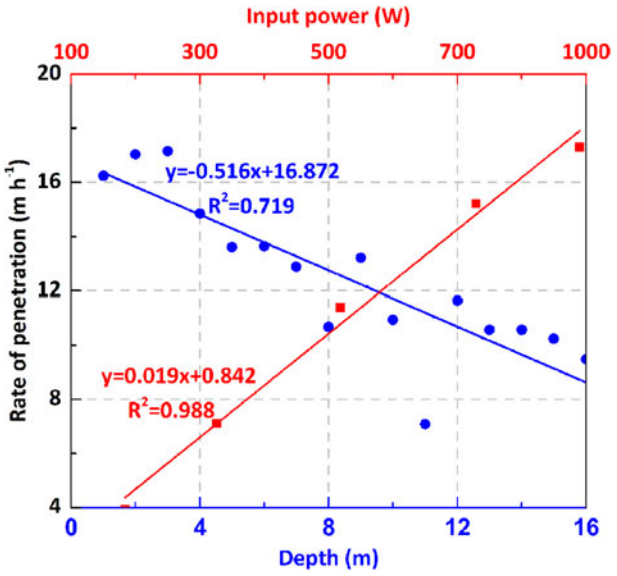

Fig. 4. Variation of the rate of penetration with input power and borehole depth.

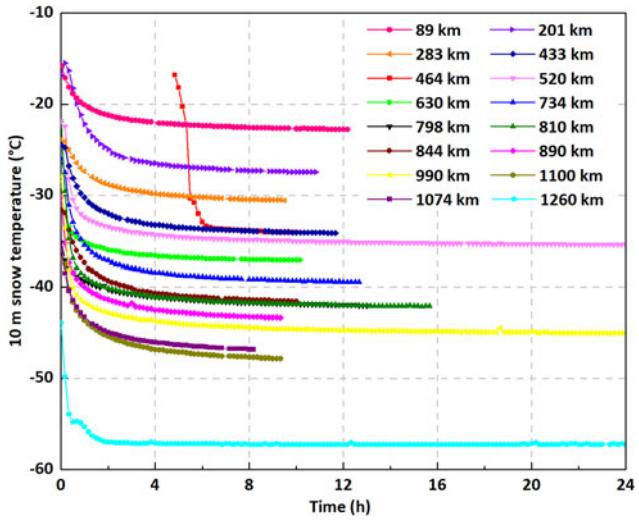

Fig. 5. Variation of 10 m snow–firn temperature with time. All the measurements are indicated in the order of distance of the sites from Zhongshan station. The temperature sensors string at site DT086 was installed into the borehole after drilling was completed for 4.8 h. The measured temperature in Kunlun station is questionable because it was not within the measurement range of the temperature chain. In the subsequent discussion, our measurement data from Kunlun station is still used, except in Figure 8.

are shown in Figure 6. In the figure, the temperature sensors are denoted as T0, T1, T2, etc., from the surface to the bottom of the borehole. Approximately 15 h was required to achieve thermal equilibrium in the borehole in the first measurement, while the time for achieving thermal equilibrium decreased to 0.7 h for the second measurement. When compared to the thermal disturbance caused by the hot-point drill, air convection in the borehole had minimal influence on the time required to achieve thermal equilibrium in the boreholes.

3.3. Theoretical estimation of annual steady-state 10 m snow–firn temperature

The Horner method is widely used for calculating static formation temperature in geothermal or oil wells based on the logged temperature of the drilling fluid (Dowdle and Cobb, 1975; Forsyth

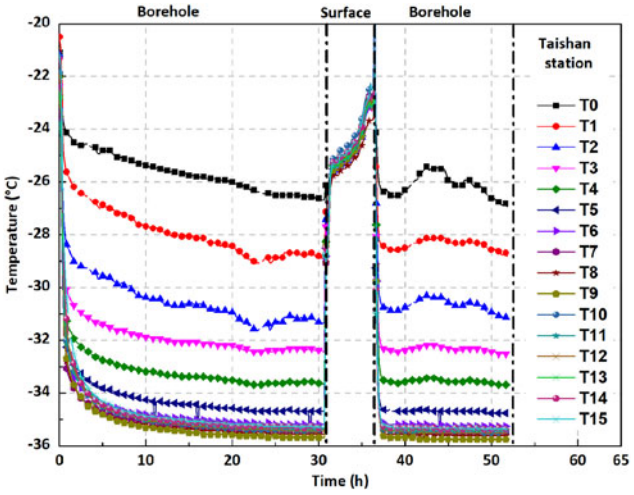

Fig. 6. Variation of borehole temperature with time in the Taishan station.

Table 3. Comparison of measured 10 m snow–firn temperature with its corrected equilibration value

No.	Sites	Measured temperature (°C)	Corrected equilibration temperature (°C)	Absolute error (°C)
1	DT086	−34.0	−35.0	1
2	DT171	−37.1	−37.5	0.4
3	DT221	−39.4	−40.0	0.6
4	DT253	−42.0	−42.5	0.5
5	DT299	−43.4	−44.2	0.8
6	DT349	−45.1	−45.3	0.2
7	DT402	−47.8	−48.7	0.9
8	Kunlun	−57.3	−57.3	0
9	DT391	−46.8	−47.7	0.9
10	DT276	−41.6	−42.2	0.6
11	DT259	−42.1	−42.5	0.4
12	Taishan	−35.4	−35.6	0.2
13	DT071	−34.1	−34.7	0.6
14	LT884	−30.6	−31.1	0.6
15	LT926	−27.4	−28.1	0.7
16	LT982	−22.8	−23.2	0.4

and Zarrouk, 2018). The method can also be used for estimating the annual steady-state snow–firn temperature in hot-point drilling when the meltwater in the pores of the surrounding snow–firn refreezes. After a minor modification of the original equation to fit hot-point drilling, the Horner method is expressed as:

$$T(\Delta t) = T_{\mathrm{i}} - m \log\left(\frac{t_{\mathrm{c}} + \Delta t}{\Delta t}\right), \quad (1)$$

where $T(\Delta t)$ is the measured borehole temperature at time Δt (°C), T_{i} is the annual steady-state snow–firn temperature (°C), m is the gradient per log cycle (°C), t_{c} is the time used for drilling (h), and Δt is the time after drilling when the borehole temperature is recorded.

The above formula was used to estimate the annual steady-state 10 m snow–firn temperature. In our case, the meltwater in the pores of the surrounding snow–firn was assumed to be completely refrozen after completing the drilling for 5 h. Therefore, in the estimation, only the measured temperature at $\Delta t \geq 5$ h was used and t_{c} was calculated based on the recorded depth and average ROP of 10 m h^{-1}.

As listed in Table 3, the corrected equilibration values of the 10 m snow–firn temperature for all the boreholes are lower than the measured values and the absolute errors between them are ≤1°C. The errors demonstrate a decreasing trend with an increase

https://doi.org/10.1017/aog.2020.87 Published online by Cambridge University Press

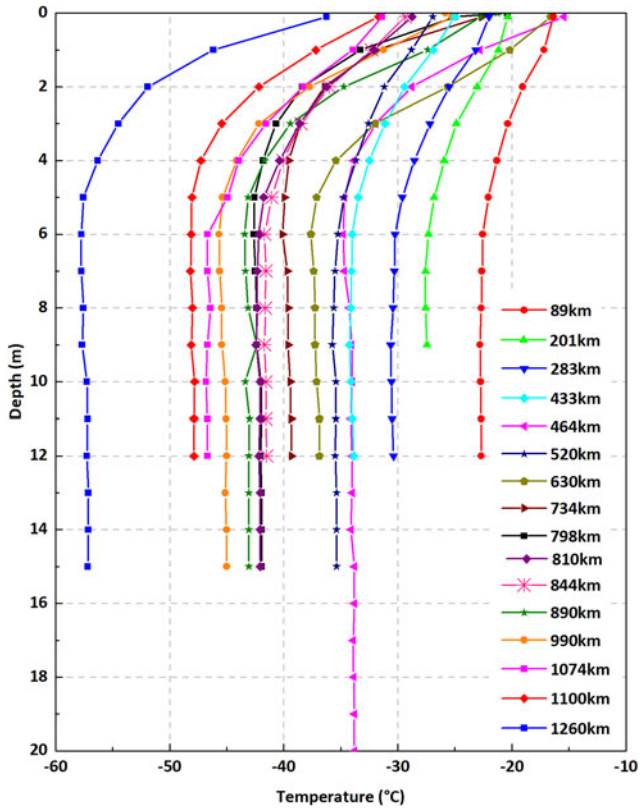

Fig. 7. Temperature distribution in the boreholes.

in the measurement time. For example, the error was 0.2°C in Taishan station with a measurement time of 31 h while it was 1°C at DT086 sites with a measurement time of 10 h. In general, the measured 10 m snow–firn temperatures were sufficiently close to the corrected equilibration temperature.

3.4. Distribution of snow–firn temperature

The temperature distribution in the 16 boreholes is shown in Figure 7 and all the boreholes are represented by their distance from Zhongshan station in the figure. In general, the temperature in each borehole first decreased with increasing depth in the upper 6–7 m and then remained almost constant until the bottom of the borehole. In the summer season in Antarctica, the surface snow temperature in daylight along the transverse changed from −15.4°C in DT086 site to −36.6°C in Kunlun station. It was also determined that the borehole temperature decreased with the increase in the distance from Zhongshan station.

Figure 8 displays the spatial distribution of measured 10 m snow–firn temperature along the Zhongshan–Dome A traverse. Here we show only our measured MAAT because the distance from Zhongshan station to measuring sites in other MAAT datasets is unknown. As the distance from Zhongshan station increased, the altitude and latitude increased, and the measured 10 m snow–firn temperature decreased. For example, the altitude in the LT982 site (89 km from Zhongshan station) increased from 1246 to 4086 m in Kunlun station while the latitude increased from 70°05′42″S to 80°25′04″S. Simultaneously, the 10 m snow–firn temperature decreased from −22.8 to −58.2°C. The

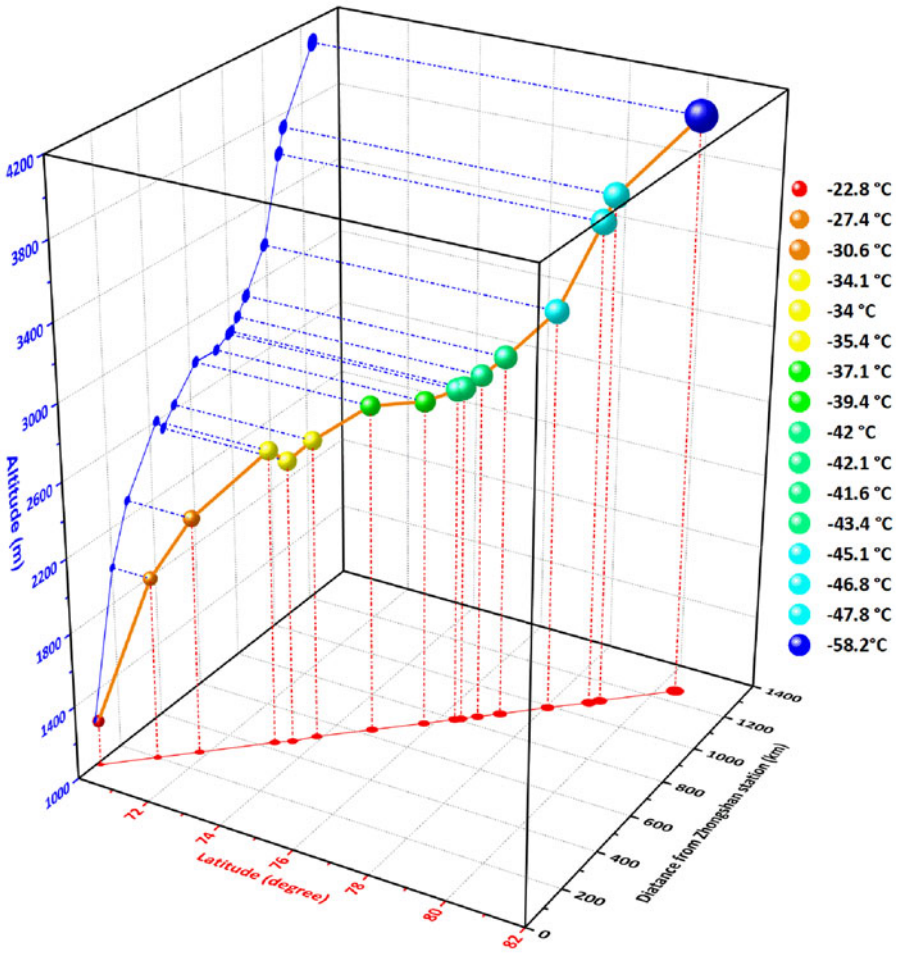

Fig. 8. Spatial distribution of measured 10 m snow–firn temperature along the Zhongshan–Dome A traverse. The 10 m snow–firn temperature in the LT926 site is replaced by the temperature measured at 9 m. The 10 m snow–firn temperature in Kunlun station measured by Chen and others (2010) was used. In the figure, the variation of latitude and altitude with the distance from Zhongshan station are shown by red and blue lines with a round dot. The MAAT is indicated by colored sphere. When MAAT is lower, the sphere has a larger size and its color is much closer to blue.

https://doi.org/10.1017/aog.2020.87 Published online by Cambridge University Press

longitudes of the 16 measurement sites were almost the same; consequently, the 10 m snow–firn temperatures at these sites were dominated by their altitudes and latitudes. To approximate the relationship between altitude A, latitude L and the 10 m snow–firn temperature T along the Zhongshan–Dome A traverse, a linear function used for describing the 10 m snow–firn temperature distribution in Antarctica peninsula was adopted (Martin and Peel, 1978; Potter and others, 1984):

$$T = a(L - 70^{\circ}) + b(A) + c, \quad (2)$$

where a, b and c are multiple regression coefficients. A standard binary regression analysis indicates that $a = -1.893°C\,deg^{-1}$; $b = -4.370 \times 10^{-3}°C\,m^{-1}$; $c = -16.659°C$. In the regression analysis, the coefficient of correlation $R^2 = 0.987$. If to account in regression analysis MAAT data given in Table 1, we obtain that $a = -1.311°C\,deg^{-1}$; $b = -6.500 \times 10^{-3}°C\,m^{-1}$; $c = -14.324°C$; $R^2 = 0.966$.

4. Conclusions

In the 2018/19 field season, along the Zhongshan–Dome A traverse, 16 boreholes were drilled using a shallow hot-point drill and the temperature distribution in the boreholes was measured using a temperature chain. Based on the drilling experience and the preliminary measurement results, the following conclusions are summarized:

(1) The shallow hot-point drill system demonstrated the ability to drill boreholes and measure the 10 m temperature in Antarctica. It was simple and light in weight for easy operation. In the expedition, the hot-point drill performed satisfactorily and it drilled more than 244 m. The ROP of the thermal head increased with input power and it was higher than $10\,m\,h^{-1}$ at a power of 890 W. During drilling, the ROP decreased with depth because of the increase in snow–firn density. In general, the hot-point drill required 1.5–2 h to drill a borehole in Antarctica for 10 m snow–firn temperature measurements.

(2) Additional dead weights or guide tubes are required to be added for the prevention of hot-point drill tilting at the opening of the boreholes. Heating the body of the hot-point drill or covering it by some other material, such as hydrophobic coating or plastic tube, was recommended. It would be better if the diameter of the thermal head was increased to 38 mm. In future, better quality cartridge heater, load sensor and motor should be used to ensure the long life of the hot-point drill and the automation of the system.

(3) When compared to a mechanical drill, the borehole drilled using the hot-point drill required more time to achieve thermal equilibrium after drilling. In our case, the time for temperature measurement was more than 12 h. The heat disturbance from the thermal head was the primary reason for the considerably long thermal equilibrium time.

(4) The Horner method was used to estimate the annual steady-state snow–firn temperature in hot-point drilling when the meltwater in the pores of the surrounding snow–firn was refrozen. Theoretically, it is possible for the estimated annual steady-state snow–firn temperature to be equal to the measured value only when the measurement time is infinity. Otherwise, it is always less than the measured snow–firn temperature.

(5) During the period of field expedition, the snow–firn temperature in each site decreased from the surface up to a depth of 6–7 m; then, it remained almost constant. The 10 m snow–firn temperature along the Zhongshan–Dome A traverse was affected by altitude and latitude. As the altitude and latitude increased from Zhongshan station to Kunlun station, the snow–firn temperature along the traverse gradually decreased.

Acknowledgements. The authors appreciate the logistic support of the 35th CHINARE and the inland team for the significant help provided during temperature measurements. This work was supported by the Ministry of Science and Technology of the People's Republic of China (Grant No. 2016YFC1400300), the National Nature Science Foundation of China (Grant No. 41706214) and the Program for Jilin University Science and Technology Innovative Research Team (Grant No. 2017TD-24).

References

Aamot HWC (1967) *Heat Transfer and Performance Analysis of a Thermal Probe for Glaciers*. USA CRREL Tech. Rep. 194.

Chen BL and 5 others (2010) A one-dimensional heat transfer model of the Antarctic Ice Sheet and modeling of snow temperatures at Dome A, the summit of Antarctic Plateau. *Science China Earth Sciences* **53**(5), 763–772. doi: 10.1007/s11430-010-0017-z.

Ding MH and 5 others (2010) Distribution of $\delta^{18}O$ in surface snow along a transect from Zhongshan Station to Dome A, East Antarctica. *Chinese Science Bulletin* **55**(24), 2709–2714. doi: 10.1007/s11434-010-3179-3.

Ding MH and 7 others (2015) Surface mass balance and its climate significance from the coast to Dome A, East Antarctica. *Science China Earth Sciences* **58**(10), 1787–1797. doi: 10.1007/s11430-015-5083-9.

Dowdle WL and Cobb WM (1975) Static formation temperatures from well logs – an empirical method. *Journal of Petroleum Technology* **27**, 1326–1330. doi: 10.2118/5036-PA.

Forsyth J and Zarrouk SJ (2018) A review of static formation temperature test evaluation methods. *Proceedings 40th New Zealand Geothermal Workshop, 14–16 November 2018, Taupo, New Zealand.*

Gillet F (1975) Steam, hot-water and electrical thermal drills for temperate glaciers. *Journal of Glaciology* **14**(70), 171–179. doi: 10.3189/S0022143000013484.

Hodge SM (1976) Direct measurement of basal water pressures: a pilot study. *Journal of Glaciology* **16**(74), 205–218. doi: 10.1017/S0022143000031543.

Ignatov VS (1960) Opyt termicheskoy prokhodki ledyanikh skvazhin na stantsii Vostok [Experiment in the thermal drilling of holes in the ice at Vostok Station]. *Informatsionny Byulleten' Sovetkoj Antark- ticheskoj ekspeditsii [Soviet Antarctic Expedition Information 7 Bulletin]* **22**, 50–52, (in Russian).

Isaksson E and 5 others (1996) A century of accumulation and temperature changes in Dronning Maud Land, Antarctica. *Journal of Geophysical Research* **101**(D3), 7085–7094. doi: 10.1029/95JD03232.

Loewe F (1970) Screen temperatures and 10 m snow temperatures. *Journal of Glaciology* **9**(56), 263–268. doi: 10.3189/S0022143000023571.

Martin PJ and Peel DA (1978) The spatial distribution of 10 m temperatures in the Antarctic peninsula. *Journal of Glaciology* **20**(83), 311–317. doi: 10.1017/S0022143000013861.

Mathews WH (1959) Vertical distribution of velocity in Salmon Glacier, British Columbia. *Journal of Glaciology* **3**(26), 448–454. doi: 10.3189/S0022143000017184.

Mock SJ and Weeks WF (1966) The distribution of 10 meter snow temperatures on the Greenland ice sheet. *Journal of Glaciology* **6**(43), 23–41. doi: 10.1017/S0022143000019043.

Morris EM and Vaughan DG (1994) Snow surface temperatures in West Antarctica. *Antarctic Science* **6**(4), 529–535. doi: 10.1017/S0954102094000799.

Potter JR, Paren JG and Loynes J (1984) Glaciological and oceanographic calculations of the mass balance and oxygen isotope ratio of a melting ice shelf. *Journal of Glaciology* **30**(105), 161–170. doi: 10.1017/S002214300000589X.

Qin DH and 8 others (2000) Primary results of glaciological studies along an 1100 km transect from Zhongshan station to Dome A, East Antarctic ice sheet. *Annals of Glaciology* **31**(1), 198–204. doi: 10.3189/172756400781819860.

Reynolds JM (1981) The distribution of mean annual temperatures in the Antarctic Peninsula. *British Antarctic Survey Bulletin* **54**, 123–133.

Satow K, Watanabe O and Nakajima C (1974) Distribution of firn temperature in Mizuho Plateau and West Enderby Land, East Antarctica. *Antarctic Record* **48**, 52–69. doi: 10.15094/00007730.

Talalay PG (2020) *Thermal Ice Drilling Technology*. Singapore: Springer Geophysics.

Thomas RH (1976) The distribution of 10 m temperatures on the Ross Ice Shelf. *Journal of Glaciology* **16**(74), 111–117. doi: 10.3189/S0022143000031464.

Ulamec S, Biele J, Funke O and Engelhardt M (2007) Access to glacial and subglacial environments in the Solar System by melting probe technology. *Reviews in Environmental Science and Biotechnology* **6**(1), 71–94. doi: 10.1007/s11157-006-9108-x.

Van Den Broeke MR and 6 others (1999) Climate variables along a traverse line in Dronning Maud Land, East Antarctica. *Journal of Glaciology* **45** (150), 295–302. doi: 10.1017/S0022143000001799.

Wang YT and Hou SG (2011) Spatial distribution of 10 m firn temperature in the Antarctic Ice Sheet. *Science China Earth Sciences* **54**(5), 655–666. doi: 10.1007/s11430-010-4066-0.

Yamada T and Narita H (1975) Snow temperatures at 10 m below the surface in Mizuho Plateau in 1972–73. *JARE Data Report* **27**, 145.

Zagorodnov V and 6 others (2012) Borehole temperatures reveal details of 20th century warming at Bruce Plateau, Antarctic Peninsula. *The Cryosphere* **6**(3), 675–686. doi: 10.5194/tc-6-675-2012.

Zagorodnov V and 7 others (2014) New technique for access-borehole drilling in shelf glaciers using lightweight drills. *Journal of Glaciology* **60** (223), 935–944. doi: 10.3189/2014JoG13J211.

Zagorodnov V, Mosley-Thompson E and Mikhalenko V (2013) Snow and firn density variability in West Central Greenland. *7th International Workshop on ice Drilling Technology, Pyle Center, University of Wisconsin, 9 September–13 September 2013, Madison, USA*, p. 64.

Zagorodnov V, Nagornov O and Thompson LG (2006) Influence of air temperature on a glacier's active-layer temperature. *Annals of Glaciology* **43**(1), 285–291. doi: 10.3189/172756406781812203.

Zeibig M and Delisle G (1994) Drilling into Antarctic ice – the new BGR ice drill. *Polarforschung* **62**(2/3), 147–150.

Zhang SK, E DC, Wang ZM, Li YS, Jin B and Zhou CX (2008) Ice velocity from static GPS observations along the transect from Zhongshan station to Dome A, East Antarctica. *Annals of Glaciology* **48**(1), 113–118. doi: 10.3189/172756408784700716.

https://doi.org/10.1017/aog.2020.87 Published online by Cambridge University Press